Multi-Photon Laser Scanning Microscopy Using an Acoustic Optical Deflector

James D. Lechleiter, Da-Ting Lin, and Ilse Sieneart
Department of Cellular and Structural Biology, University of Texas Health Science Center at San Antonio, San Antonio, Texas 78229 USA

ABSTRACT Multi-photon laser scanning microscopes have many advantages over single-photon systems. However, the speed and flexibility of currently available multi-photon microscopes are limited by the use of mechanical mirrors to steer pulsed radiation for fluorophore excitation. Here, we describe the multi-photon adaptation of a confocal microscope that uses an acoustic optical deflector (AOD) for beam steering. AODs are capable of very rapid scanning and, in addition, offer the flexibility of zooming, panning, and being adjustable for slow image acquisition. Because of the highly dispersive nature of AODs, pulsed radiation must be temporally compressed by introducing negative dispersion into the beam path. More critically, pulsed radiation must also be spatially compressed by introducing lateral dispersion into the beam path. This was accomplished by using two prisms in the external beam path and by introducing a third prism element subsequent to the AOD. The end result is an AOD-based multi-photon microscope that is capable of rapid imaging of physiological events as well as slow detection of weakly fluorescent biological samples.

INTRODUCTION

The underlying principle of multi-photon laser scanning microscopy is that the fluorophore must simultaneously absorb multiple photons of typically one-half to one-third the energy required for single-photon excitation (Denk et al., 1990). The probability for such an event occurring is only significant at the plane of focus, where photon flux is the highest. Thus, out-of-plane fluorescence does not occur and thin optical sections are automatically generated without the use of confocal point detection of de-scanned fluorescence. The absence of a confocal pinhole also increases the sensitivity of light detection, because all of the in-focus fluorescent light can be collected without contamination from out-of-focus imaging planes. Image contrast is greatly increased, and photobleaching and phototoxicity are dramatically reduced because fluorophores outside the imaging plane are not excited. Finally, the wavelength of light used for excitation is in the infrared range (~700–1000 nm), where biological preparations are not as absorbent. Consequently, images can be collected at greater depths into cells or tissues. For all of these reasons, multi-photon laser scanning microscopy is ideal for in vivo imaging (Centonze and White, 1998; Xu et al., 1996).

A satisfactory probability of nearly simultaneous absorption of multiple photons requires pulsed radiation, which is characterized by its pulse duration (e.g., 100 fs) and central wavelength (e.g., 800 nm) as well as the spectral spread around the central wavelength at full-width half-maximal (FWHM) power (e.g., 10 nm). The spectral spread of pulsed radiation has so far limited the optical design of multi-photon imaging systems. In particular, galvanometer or resonant mirrors have been used to steer the laser beam, because these optical elements reflect light in a wavelength-independent manner. However, galvanometric mirrors are relatively slow, and resonant mirrors do not have the flexibility to scan at slower speeds or to change zoom and pan the image. Beam steering with AODs overcomes these limitations, offering a broad range of flexible scanning speeds from very rapid (~30–120 frames/s) to slow (~1 frame/s), without sacrificing the ability to zoom or pan an object. However, AODs also introduce significant optical dispersion, which has until now prevented their incorporation into multi-photon imaging systems. Specifically, AODs usually use the highly dispersive material tellurium dioxide (TeO_2), which causes temporally dispersion or broadening of radiation pulses. In addition, the angle of deflection by these optical elements is wavelength dependent, introducing additional complications. Consequently, pulsed radiation that is refracted by these optical elements is distorted not only temporally, but also spatially, which significantly lowers the probability of simultaneous absorption of multiple photons. In this paper, we present optical corrections for confocal laser scanning microscopes using AODs that permit their adaptation for multi-photon imaging.

METHODS

Optical layout

A schematic diagram of the physical layout and optical components used to adapt the NORAN OZ confocal microscope for multi-photon imaging is presented in Fig. 1 *A*. Pulsed radiation is generated by a Ti-sapphire laser (Mira 900-F, Coherent Lasers, Santa Clara, CA) pumped with a solid-state laser (VERDI 5W, Coherent Lasers). For the work described in this manuscript, the emerging beam of pulsed radiation was centered at wavelength 800 nm and

Submitted February 12, 2002, and accepted for publication June 5, 2002.
Address reprint requests to Dr. James D. Lechleiter, Department of Cellular and Structural Biology, University of Texas Health Science Center at San Antonio, 7703 Floyd Curl Drive, San Antonio, TX 78229-3900. Tel.: 210-567-6254; Fax: 210-567-6781; E-mail: lechleiter@uthscsa.edu.

0006-3495/02/10/2292/08 $2.00

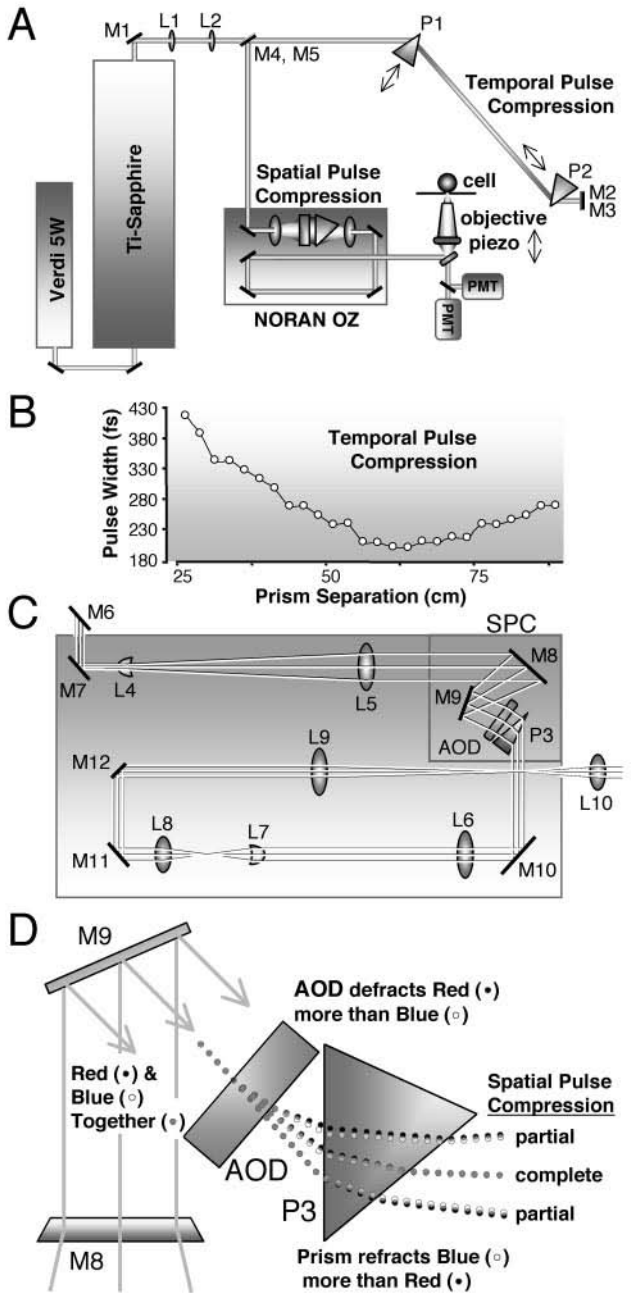

FIGURE 1 (*A*) Schematic diagram of the physical layout and optical components of the multi-photon adapted NORAN OZ confocal microscope. A Verdi 5-W laser is used to pump a MIRA 900-F Ti-sapphire laser to generate pulsed radiation (Coherent Lasers). Steering mirrors (M), lenses (L), and prisms (P) are numbered, and a description of their function is provided in the text. Temporal pulse compression is added between prisms P1 and P2. Spatial pulse compression is added within the NORAN OZ scan box. External photomultipliers (PMT) are used for non-descanned detection of fluorescence. The objective lens was mounted on a piezoelectric drive to permit rapid *xz* and *xyz* scanning. (*B*) Plot of the pulse width of the radiation source as a function of the separation between prisms P1 and P2. Pulse width was measured with an autocorrelator (Mini, APE) at the back aperture of the microscope objective. (*C*) Schematic layout of the modified optical components within the NORAN OZ scan box. These components are numbered as in *A*, and their function is described in the text. The added elements used for spatial pulse compression (SPC) are framed in the upper right corner. Note that the orientation of the components has been altered to illustrate the beam path, and it is viewed from the right side of the scan box. (*D*) Detail of the SPC as seen from L5 within the scan box. A single beam of pulsed radiation through the AOD and prism element P3 is presented. Before the AOD, different wavelengths within the pulsed radiation travel together (*gray filled circles*). The AOD defracts red light (*black filled circles*) more than blue (*white filled circles*). Lateral pulse spreading is greatest at the largest diffraction angle. The critical adaptation to the NORAN OZ resides in prism element P3, which compresses the pulses by refracting blue light more than red. Note that spatial pulse compression is complete at the center of the scan, whereas partial pulse compression is also achieved at the edges.

had a pulse width of ~180 fs, as measured by a laser spectrum analyzer (E200 LSA, IST-Rees, Horseheads, NY) and a pulse autocorrelator (Mini, APE, Berlin, Germany). At FWHM power, the bandwidth was ~10 nm. The emerging beam is initially turned by a mirror (M1) and collimated with a ×2 beam expander (L1). Collimation was further extended by the addition of a long-focal-length plano-convex lens (L2).

RESULTS

Temporal dispersion

Group velocity dispersion occurs because materials with shorter wavelengths of light have higher refractive indices than longer wavelengths of light (Denk et al., 1995). Consequently, blue light lags behind red light after each optical element and radiation pulses are temporally broadened (Bor, 1988). When a radiation pulse of ~180 fs was passed through the NORAN OZ confocal scanning box (NORAN Instruments, Middleton, WI), the pulse was temporally broadened to ~920 fs. The final pulse width was measured at the back aperture of the objective where the pulse power was 40 mW. The large amount of dispersion was due primarily to the AOD, which is composed of TeO_2. We offset this positive dispersion by preconditioning the pulse with negative dispersion using the method originally described by Fork and co-workers (Fork et al. 1984) and later simplified by Soeller and Cannell (1996). In brief, prisms are used to compensate for the slower velocity of shorter wavelengths by forcing the longer-wavelength components of the pulse to traverse longer path lengths through the dispersion prism elements. As shown in Fig. 1 *A*, the pulsed beam is refracted through two prisms (P1 and P2) and then returned through the same prisms with two mirrors (M2 and M3). P1 and P2 were adjusted to Brewster's angle of incidence to minimize reflection losses from prism surfaces. The apex of P1 was inserted into the beam path sufficiently to refract the entire beam to P2. P1 spatially distorts the pulse profile because shorter wavelengths are

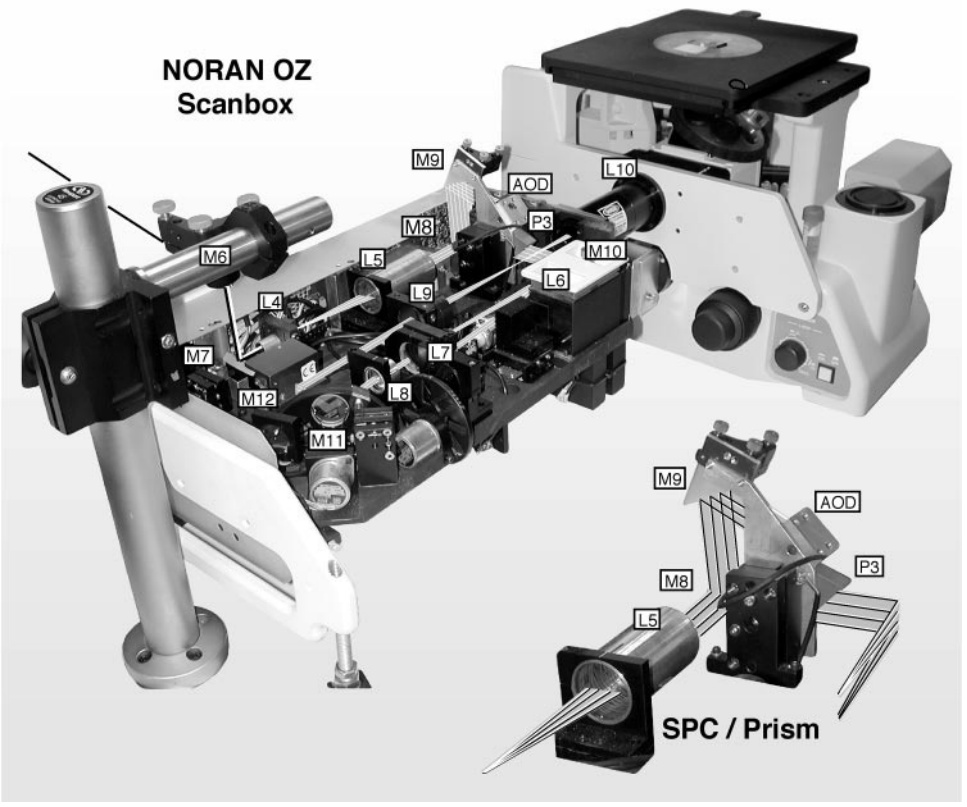

FIGURE 2 Photographic layout of the modified optical elements with the NORAN OZ scan box. The M6 mirror is mounted on a 45° adaptor (9920, New Focus), held in a center mount holder (9807, New Focus) and clamp (9141, New Focus) that is attached to a 6-inch pedestal (9962, New Focus). The pedestal, in turn, was attached to a rod (model 45, Newport) and clamp (340-RC, Newport) assembly. Modified mirror (M) and lens (L) elements are labeled and described in the text. L6 and M10 are not visible in the photograph. However, their positions and mounts were not changed. The inset (*lower right*) shows a higher magnification of the modification near the SPC/prism assembly. A custom aluminum mount was created to hold mirror M9, the AOD, and prism P3. The AOD and P3 were attached to the aluminum mount with epoxy. A miniature kinematic mirror mount (U50-A, Newport) was used to attach M9.

refracted more than longer ones. The apex of P2 is inserted into the beam path sufficiently to refract the beam to M2. This results in a longer dispersive path length for the longer-wavelength components, because they are refracted through P2 further from the apex, thereby adding negative dispersion to the radiation pulses. M2, in combination with M3, are adjusted to return the beam vertically displaced by ~15 mm through the same prisms. The amount of negative dispersion can be adjusted by varying the distance between P1 and P2. A prism separation of ~65 cm was sufficient to fully compensate for the positive dispersion introduced by the AOD optical element, resulting in a final pulse width of ~200 fs (Fig. 1 *B*).

Another set of mirrors (M4 and M5; Fig. 1) are used to steer the preconditioned radiation beam toward M6, which is positioned just above the NORAN OZ scan box (Figs. 1 *C* and 2; Table 1). A dichroic mirror (M7) was positioned inside the scan box, just before the first cylindrical NORAN lens (L4, Figs. 1 *C* and 2). M6 and M7 are adjusted to align the pulsed beam within the scan box.

Modifications to the NORAN OZ scan box

To optimize the NORAN OZ scan box for multi-photon imaging, the existing mirrors and lenses were replaced with new optical elements. These optical elements avoid significant power loss and pulse distortion in the infrared range. New mirror blanks were obtained from the optical supply company of NORAN Instruments (Republic, Inglewood, NJ), and subsequently coated to efficiently reflect visible and infrared wavelengths (triple stack, visible 450–6 5 0 nm, ultrafast 720–850 nm, S&P polarized; CVI Laser Corp.). Specifically, the following mirrors were exchanged for their respective originals: the first mirror after the AOD, M10; the mirror in the dichroic filter wheel, M11; and the galvanometer mirror, M12. The single mirror just before the AOD was replaced with two new mirrors, M8 and M9 (Figs. 1, *C* and *D*, and 2). Two beam steering mirrors subsequent to L9 were eliminated. The lenses within the scan box were also replaced with new optics that were coated for efficient transmission in the infrared range. More specifically, the original lenses were exchanged with the negative cylindrical

TABLE 1 Commercial sources of optical elements

Element	Catalog number	Source
L1	CWBX-7.0-2X-670-1064	CVI Laser Corp. Albuquerque, NM
L2	PLCX-25.4-1545.0-C-670-1064	CVI Laser Corp.
L4	01LCN124/073	Melles Griot, Irvine, CA
L5 and L6	01LAO149/073	Melles Griot
L7	01LCP125/073	Melles Griot
L8	01LAO111/073	Melles Griot
L9	01LAO135/073	Melles Griot
L10	01LAO189/073	Melles Griot
P1 and P2	IB-21.6-60.6-SF10	CVI Laser Corp.
M1	TLM2-800-45-1025	CVI Laser Corp.
M2 and M3	TLM2-800-45-0537	CVI Laser Corp.
M4 and M5	TLM2-800-45-1025	CVI Laser Corp.
M6	SWP2-R700-900-TVIS-45-1025	CVI Laser Corp.
M7	SWP2-R700-900-TVIS-45-1025	CVI Laser Corp.
M8	370A130257	Republic, Inglewood, NJ
M9	370A136256	Republic
M10	TLM2-800-45-1025	CVI Laser Corp.
M11	370A129941	Republic
M13	SWP2-R700-900-TVIS-45-1025	CVI Laser Corp.

lens, L4; the AOD input/output lenses, L5 and L6; the positive cylindrical lens, L7; the collimating lens, L8; and the focusing lens, L9. After these modifications were introduced into the scan box, the power throughput could be adjusted to transmit ~10–12% of the incident power of the pulsed radiation at M6. For example, with an incident power of 700 mW, the power measured at the back aperture of the objective lens was 72 mW. The low transmission efficiency is due primarily to the loss of power at the AOD, which is characteristic of its design. AODs generate diffraction patterns of light consisting of a zero-order band as well as higher-order diffraction bands. The position of the zero-order band is fixed, and only the energy that is diffracted into the first-order band is used for imaging. By applying acoustic waves to the TeO_2 crystal, the spacing of the AOD diffraction grating is changed, thereby altering the position of the first-order band. Thus, AODs are inherently inefficient power transmitters because only a fraction of the incident power is diffracted into the first-order band.

Compensation for AOD-induced pulse spreading

The position of the first-order diffraction band is dependent on the wavelength of light that is diffracted by the AOD. Longer wavelengths are diffracted further away from the fixed zero-order band. Because pulsed radiation is composed of multiple wavelengths, AODs spread the first- and higher-order diffraction bands in the lateral direction. The magnitude of lateral spreading also increases with the angle of deflection (Fig. 1 *D*). Prisms refract light in a wavelength-dependent manner, inversely to the AODs. We compensated for this distortion by inserting a custom prism (P3) subsequent to the AOD, resulting in a spatial compression of the pulses (Figs. 1 *D* and 2). Typically, the FWHM power of the pulse radiation that we use is 10 nm or less. Thus, we conservatively estimated the required amount of compensation for a 20-nm spectral spread by calculating the theoretical deflection differences between 790 and 810 nm at the center of the AOD scan. The wavelength-dependent angle of diffraction expected from the AOD in radians was calculated using the following equation:

$$\theta_\beta = \lambda f_o / 2V, \quad (1)$$

where θ_β is the angle of deflection by the AOD, λ is the wavelength of light to be deflected, f_o is the acoustic mod-

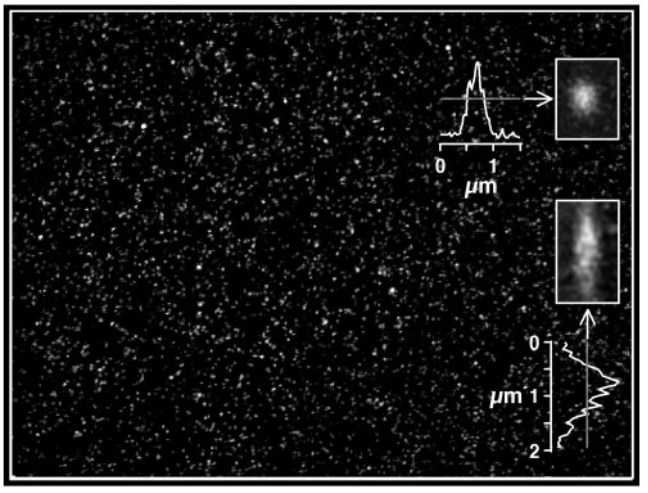

FIGURE 3 Full-field image of fluorescent beads collected with the multi-photon adapted NORAN OZ confocal microscope. The fluorescent beads were plated on a glass coverslip as described in the text and scanned at zoom 1 using a 60 × 1.2 NA water immersion objective (C-Apo, Nikon). The insets show images of a single fluorescent bead in the *xy* (*top*) and *xz* (*bottom*) planes collected at zoom 5.

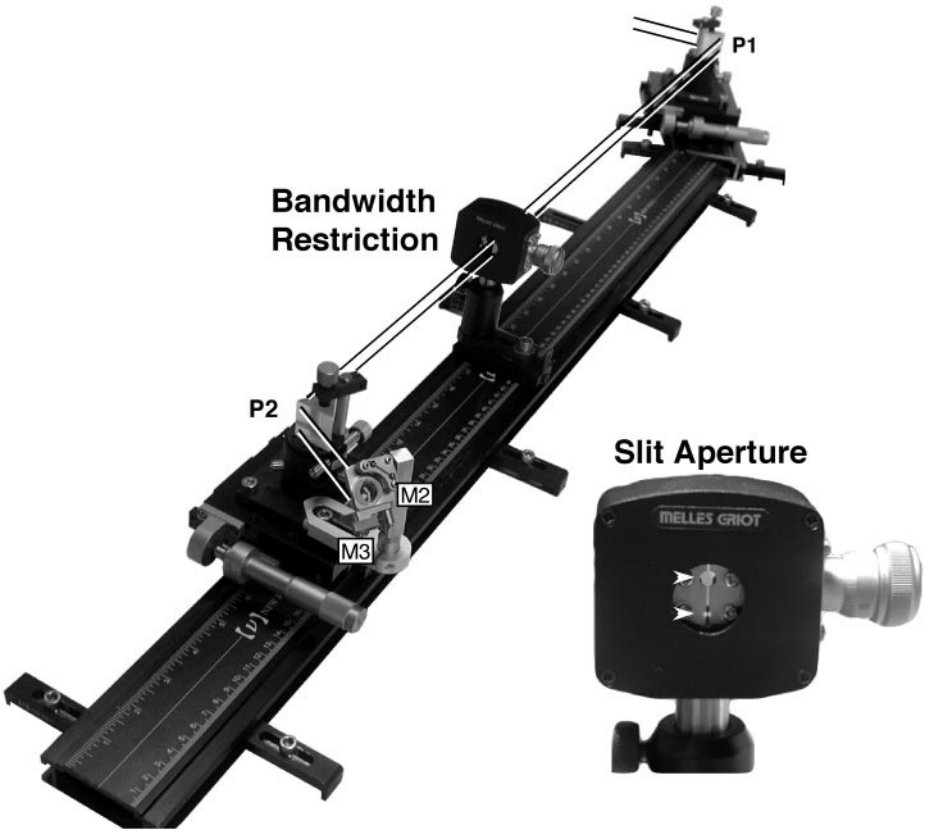

FIGURE 4 The photographic layout of the external pulse compressor used for temporal pulse dispersion compensation. Bandwidth restriction of the pulse is achieved by placing an adjustable slit aperture (07 SLT 001, Melles Griot) between prisms P1 and P2. At this location, the light is spread laterally in a wavelength-dependent manner. By closing the slit, the pulse bandwidth can be restricted. The inset on the lower right shows a high magnification of the slit aperture in the partially closed position. The initial beam, from P1 to P2, passes unobstructed through a hole that was machined in the slit (*upper arrowhead*). The partial restriction of the returning beam can be seen as a white reflection on the edges of the slit (*lower arrowhead*).

ulation frequency applied to the AOD, and V is the velocity of the acoustic wave traversing the AOD crystal. For an AOD composed of TeO_2, $V = 4322$ m/s and 200 MHz $< f_o <$ 400 MHz (NORAN Instruments). At 300 MHz (center of the scan), the AOD spreads a 20-nm pulse ($790 < \lambda < 810$ nm) $\sim 0.04^o$.

The thin prism approximation was used to calculate the apex angle of the prism required to merge the 790- and 810-nm wavelengths as follows:

$$\delta = (n - 1)\alpha, \tag{2}$$

where δ is the angle of deflection, n is the refractive index, and α is the angle at the apex of the prism. The calculated prism apex angle for SF11 material (Schott Glass Co.) was 48^o. This prism was custom ordered (30 × 12 mm clear aperture, ultrafast coating 700–900 nm, flatness one tenth wave at 546 nm over the clear aperture of both surfaces, 60–40 scratch and dig, 12 mm thickness; CVI Laser Corp.) and mounted after the AOD (Figs. 1 *D* and 2). The AOD/prism assembly was positioned such that the light emerging from the prism was co-aligned with the continuous wavelength optical path from M10 onward. The laser beam was steered into the AOD with the use of M8 and M9 (Figs. 1 *D* and 2). To maintain efficient power transfer through the crystal, the AOD input lens, L5 ($f = 160$ mm), was mounted closer to the AOD so that input light would still be focused onto the TeO_2 surface.

Modifications to the microscope

The temporally and spatially compensated beam of pulsed radiation was directed into an inverted microscope (Nikon TE200) through the side of the Nikon fluorescent boat. The Nikon tube lens was replaced with an ultrafast lens, L10. A shortpass, ultrafast mirror M13 was used to direct the excitation beam into a 60 × 1.2 N.A. water objective. Fluorescent non-descanned light was detected with external photomultipliers (Fig. 1 *A*). To this end, the internal transmitted and reflection photomultipliers were removed from the NORAN OZ scan box and remounted on a custom holder attached to the side camera port. The custom holder was also designed to receive a standard Nikon fluorescent filter cube to separate fluorescent signals. Immediately before the photomultipliers, a lens ($f = 100$ mm) was placed to focus all of the collected fluorescent light onto the photomultipliers. The position of this lens was empirically adjusted to provide maximum fluorescence intensity across the entire scanned image.

Optical performance

Fluorescent beads (100 nm; Molecular Probes, Eugene, OR) were imaged to test the optical performance of the modified multi-photon NORAN OZ microscope. The beads were suspended in water, transferred to a glass coverslip, and allowed

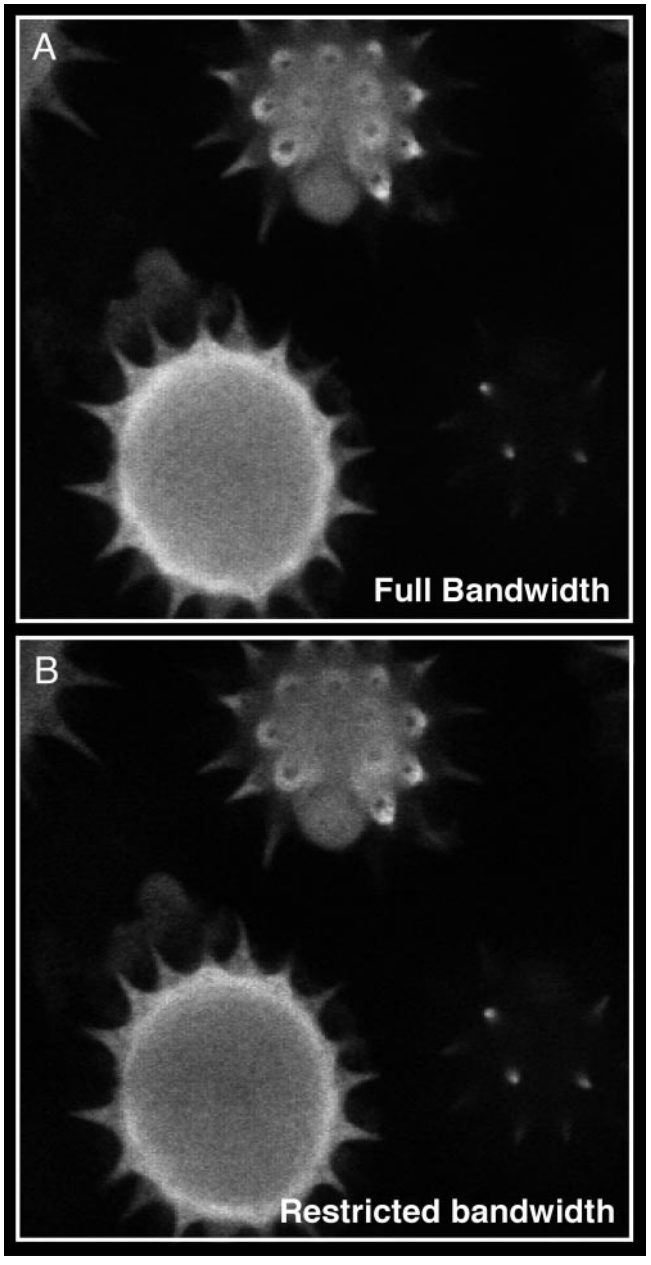

FIGURE 5 Bandwidth restriction does not improve image resolution. (*A*) Mixed pollen grains were scanned at zoom 1 at full pulse bandwidth without the slit aperture. (*B*) The same field of pollen grains was scanned a second time after the slit aperture was partially closed (Fig. 4 *inset*). The laser power was increased to provide the same image brightness shown in *A*. The photomultiplier gain setting was not changed.

to air dry so that they tightly adhered to the coverslip. Before imaging, water was added to the coverslip. This procedure allows the point-spread function to be measured without movement. A full-field image (zoom 1, Nikon ×60 water immersion objective, 1.2 NA, excitation wavelength 800 nm) is presented in Fig. 3. A single bead that was imaged at high resolution (zoom 5, center of field) and sectioned in 0.1-μm steps is presented in *xy* cross section and *xz* projection (Fig. 3 *insets*). The FWHM values for the *xz* and *xy* line plots of this bead are 0.33 and 1.1 μm, respectively.

The AOD lateral pulse dispersion can be fully compensated at the center of the scan by the addition of the corrective prism P3. However, the theoretical spatial pulse compression provided by the prism element is not uniform across the entire scan of the AOD. At minimal pulsed beam deflection, the corrective prism refracts blue light more than red light, leading to an over-compressed, blue-shifted spreading of the pulse. Likewise, at maximal pulsed deflection, the prism also provides partial compensation, resulting in an under-compressed, red-shifted pulse of radiation (Fig. 1 *D*). The ability of this microscope to excite fluorophores with pulsed radiation across the entire scan indicated that the partial pulse compression at the edges was below the diffraction limit of light (Fig. 3). To test whether a reduction in the spectral bandwidth of the pulsed radiation could further increase image resolution, we positioned a mechanical slit between the prisms located in the external pulse compressor (Figs. 1 *A* and 4). Between these prisms, light is spectrally separated. By partially closing the slit, the longest and shortest wavelengths of the radiation pulses could be blocked. We imaged a field of mixed pollen grains (catalog item 30–4264, Carolina Biological Supply Co.) with the slit fully open and compared the resolution with the slit partially closed. Laser power was increased to produce the same level of fluorescence intensity of the pollen grains without changing the photomultiplier gain. We observed no significant difference in image quality as a result of narrowing the bandwidth (Fig. 5). These results demonstrate that spatial pulse compression provided by the P3 prism is within the diffraction limit of light across the entire imaging field. We also tested the performance of the multi-photon-adapted AOD microscope at multiple excitation wavelengths, because the P3 prism was designed to compensate for lateral dispersion at 800 nm. To accomplish this, we imaged the same field of pollen grains at 10 different excitation wavelengths ranging from 720–880 nm, in 20-nm increments. Values outside this range were not tested because our optics were not coated for those wavelengths. The results are presented in Fig. 6. We found that the P3 prism provided good lateral compression from 780–880 nm, resulting in excellent image quality. Optimal correction appeared to be centered near 840 nm, as indicated by the enlarged pollen grain spine at the edge of the imaging field (Fig. 6 *insets*). Excitation wavelengths below 780 became progressively worse, resulting in poor optical sectioning and image quality at 760, 740, and 720 nm. Replacement of P3 with an alternative prism designed specifically for these shorter wavelengths would likely enhance the image quality. We also examined two-photon excitation power as a function of scan position in a uniform field of fluorescent plastic (λ 457–528-617, gift of Delta Vision from Applied Precision). Excitation is essentially uniform across ~60% of the field at 800 nm and ~50% of the field at 840 nm (Fig. 6 *B*). Small

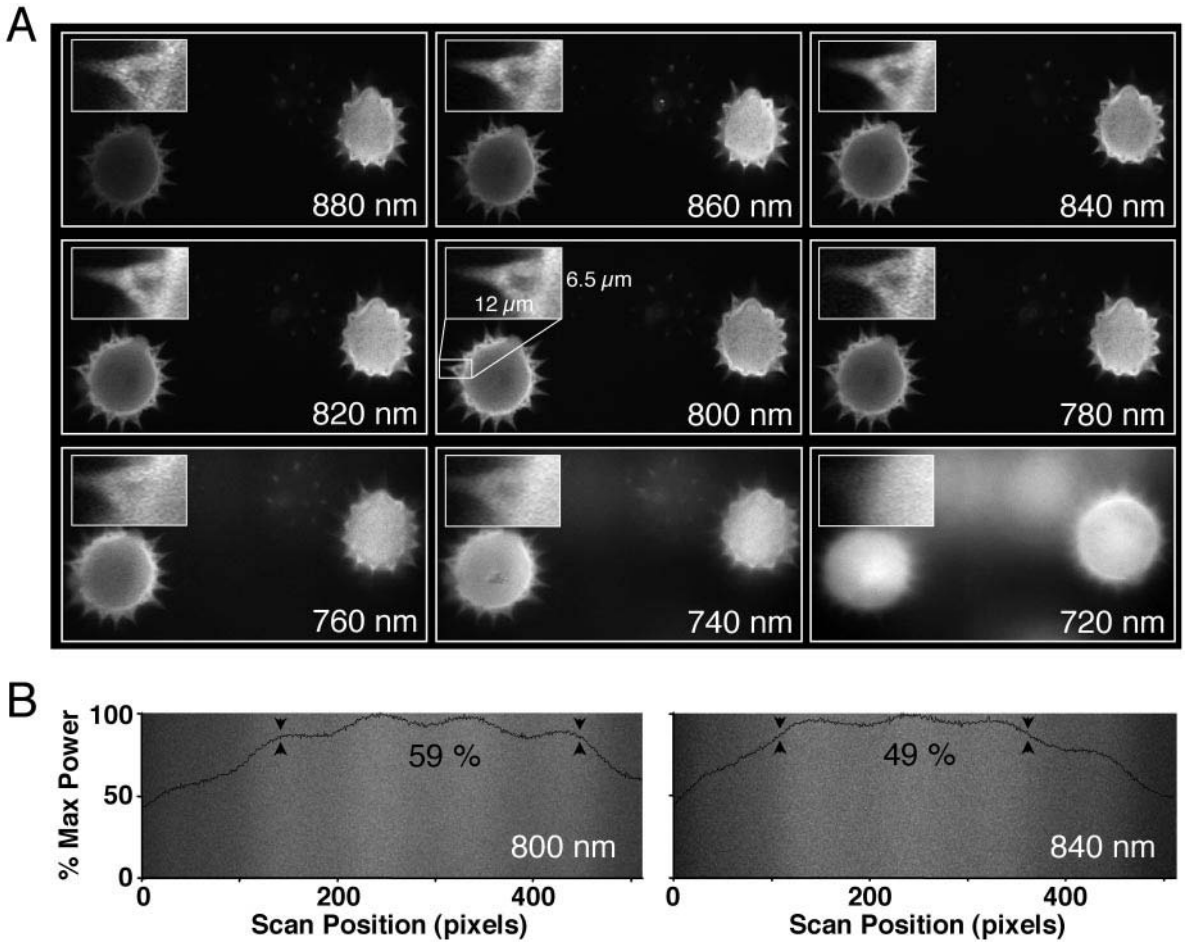

FIGURE 6 Wavelength-dependent excitation of pollen grains using the multi-photon adapted NORAN OZ microscope. (*A*) The same field of pollen grains (125 × 65 μm; 512 × 266 pixels) was excited with pulsed radiation at each of the indicated wavelengths. The inset of each panel shows a higher magnification of a single spine for each wavelength. The original location of this spine is marked by a small white rectangular frame (12 × 6.25 μm) on the left pollen grain of the 800-nm panel. Each image represents an average of eight images scanned at the slow setting of 200 ns (pixel dwell time). Excitation power was 14 mW (20% of 72-mW maximum), measured at the back aperture of the objective. (*B*) Fluorescent images (156 × 512 pixels; zoom 1) of a uniform field of fluorescent plastic (λ 457–528-617, gift of Delta Vision from Applied Precision) excited at 800 and 840 nm. Intensity profiles (*black traces*) for each image are normalized to 100% fluorescence at the center of the field. Double arrows indicate the point at which excitation power drops to 90% of maximum. The percentage of the field above 90% is indicated between the double arrows for each image.

sinusoidal variations in image intensity were inherent in our AOD scanner (NORAN Instruments, personal communication, 2002). Note that the image quality at the edge of the field was maintained, even though excitation power was reduced to ~50% of maximum (Fig. 6 *A*).

Finally, to demonstrate the dynamic imaging capabilities of this multi-photon microscope, we imaged inositol triphosphate (IP_3)-induced Ca^{2+} wave activity in a *Xenopus* oocyte overexpressing a sarcoendoplasmic reticulum Ca^{2+} ATPase (SERCA2b) (John et al., 1998). Imaging of Ca^{2+} activity was performed with the Ca^{2+} indicator dye, Oregon Green 488 BAPTA-2 (single-photon absorbance peak at ~ 494; Molecular Probes). The final dye concentration was 25 μM and was excited by two-photon absorption at 810 nm (Fig. 7). The tip of a spiral wave that was induced by a bolus injection of IP_3 (6 μM final) was imaged (zoom 1512 × 480 pixels).

DISCUSSION

We have described an optical adaptation of a NORAN OZ confocal scanning microscope for use as a multi-photon microscope. The key optical component that is required for this adaptation is the placement of a prism just subsequent to the AOD. This prism serves to spatially compress pulsed radiation and compensate the lateral dispersion introduced by the AOD. Our tests demonstrated that a single-prism design provides excellent optical correction for at least a 100-nm range of excitation wavelengths (780–880 nm; Fig. 6), even though the spatial compression of the pulsed radiation was designed for a single wavelength. In addition, we found that fluorophores could be excited across the entire imaging field, even though a single-prism correction is not symmetrical across the scan. Two factors may contribute to

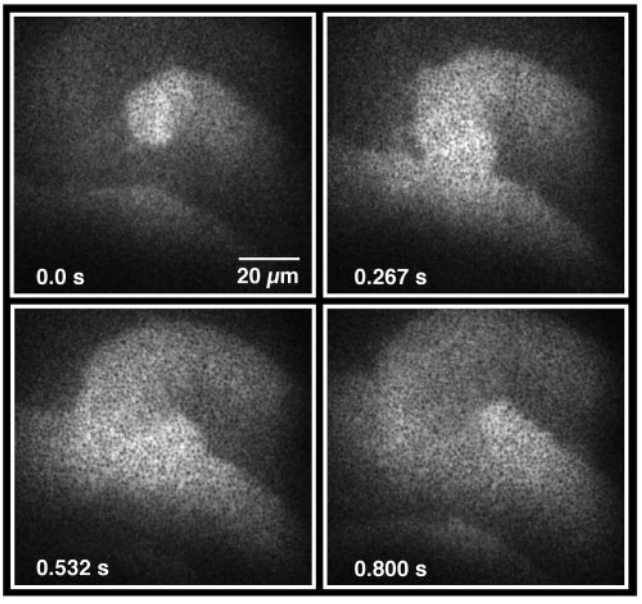

FIGURE 7 Spiral Ca^{2+} wave activity imaged with the multi-photon adapted NORAN OZ microscope. IP_3 injection (6 μM final) induced intracellular Ca^{2+} release in a *Xenopus* oocyte overexpressing the Ca^{2+} pump, SERCA 2b. Oregon Green 488 BAPTA-2 was used as the fluorescent Ca^{2+} indicator at a final concentration of 25 μM. Each panel is a full-field image (512 $\times$ 480 pixels) collected with a 60 $\times$ 1.2 NA water immersion objective at zoom 1. The numerous small black dots are cytoplasmic vesicles that exclude dye.

the efficacy of a single-prism correction. First, the pulse bandwidth is relatively narrow (e.g., ~10 nm at FWHM) and as a consequence, the under- and overcompensated pulse spreading may be below the diffraction limit of light at the specimen plane. Second, AODs act as natural bandwidth filters. For maximum diffraction efficiency, light must enter the TeO_2 crystal at the Bragg angle. In the case of a spectrally wide pulse, only the central wavelength would match the correct angle for maximum efficiency, whereas the side wavelengths would be attenuated. The end result would be a pulse with less bandwidth and, hence, the need for less pulse correction across the scanning field. Irrespective of the precise underlying mechanism(s), the single-prism element clearly provides ample compensation for confocal laser scanning microscopes that use AODs for beam steering to provide multi-photon excitation at a range of wavelengths and across the entire imaging field.

Ultimately, the major limitation of high-speed imaging is not scanning speed, but signal strength. Lack of photons per pixel sets the imaging speed limit. Other imaging systems with rapid scanning capabilities are currently available for multi-photon imaging. However, these systems are restricted to high-speed scanning, which can be problematic when trying to image weak fluorescent signals. Under these conditions, the only option to record an image with acceptable signal-to-noise levels is to average the fluorescent signal. A significant advantage of AOD scanning technology over fixed rapid imaging systems is the ability to slow scanning speeds, thereby increasing the pixel dwell time and, in turn, the sensitivity of the system without the need to signal average. AOD technology also provides excellent control of the scanning beam. With appropriate software, the end user could excite and simultaneously monitor the fluorescent signal from multiple sites within the imaging field. Zooming and panning of the image are also possible. Finally, the necessity to de-scan fluorescent signals in confocal imaging was previously considered to be a major limitation of AOD-based beam steering. AOD-based systems required a slit instead of a pinhole to eliminate out-of-focus fluorescence and resulted in significant loss of spatial resolution. Multi-photon imaging eliminates this problem because the fluorescent signal does not need to be de-scanned for optical sectioning. Non-descanned fluorescence can be detected with external photodetectors, because only the in-focus fluorophores are excited by multi-photon absorption. The use of external detectors placed close to the objective also increases the sensitivity of the system because of the ability to collect scattered fluorescence as well as the elimination of the pinhole. For all of these reasons, AOD-based multi-photon imaging represents a significant breakthrough in imaging technology. End users can now take advantage of multi-photon imaging without sacrificing their experimental requirements for speed, flexibility of image acquisition, or spatial resolution.

We thank Dr. P. Camacho for her insightful comments and critique of the manuscript.

This work was funded by National Institutes of Health grant R01 GM48451 to J.D.L.

REFERENCES

Bor, Z. 1988. Distortion of femtosecond laser pulses in lenses and lens systems. *J. Modern Opt.* 35:1907–1918.

Centonze, V. E., and J. G. White. 1998. Multiphoton excitation provides optical sections from deeper within scattering specimens than confocal imaging. *Biophys. J.* 75:2015–2024.

Denk, W., D. W. Piston, and W. W. Webb. 1995. Two-photon molecular excitation in laser-scanning microscopy. *In* Handbook of Biological Confocal Microscopy. J. B. Pawley, editor. Plenum Press, New York. 445–458.

Denk, W., J. H. Strickler, and W. W. Webb. 1990. Two-photon laser scanning fluorescence microscopy. *Science.* 248:73–76.

Fork, R., O. Martinez, and J. Gordon. 1984. Negative dispersion using pairs of prisms. *Opt. Lett.* 9:150–152.

John, L. M., J. D. Lechleiter, and P. Camacho. 1998. Differential modulation of SERCA2 isoforms by calreticulin. *J. Cell. Biol.* 142:963–973.

Soeller, C., and M. B. Cannell. 1996. Construction of a two-photon microscope and optimisation of illumination pulse duration. *Pflugers Arch.* 432:555–561.

Xu, C., W. Zipfel, J. Shear, R. Williams, and W. Webb. 1996. Multiphoton fluorescence excitation: new spectral windows for biological nonlinear microscopy. *Proc. Natl. Acad. Sci. U.S.A..* 93:10763–10768.